Development of predictive models of π-facial selectivity; a critical study of nucleophilic addition to sterically unbiased ketones

U. Deva Priyakumar,[a] G. Narahari Sastry[a],* and Goverdhan Mehta[b],*

[a]Molecular Modelling Group, Organic Chemical Sciences, Indian Institute of Chemical Technology, Hyderabad 500 007, India
[b]Department of Organic Chemistry, Indian Institute of Science, Bangalore 560 012, India

Abstract—Quantum chemical calculations at B3LYP/6-31G* and semiempirical levels have been performed on a series of sterically unbiased ketones, where facial differentiation during nucleophilic additions is electronically induced through distal functional groups. The face selectivity data for fifty-four substrates representing nine different skeleta were computed and compared with the available experimental data on thirty-eight of them. The predictive abilities of various computational methods such as, charge model, hydride model, LiH transition state model, Cieplak hyperconjugation effect estimated by NBO analysis and the cation complexation model have been evaluated. A comparison of the computed and experimental face-selectivity data indicates that the hydride model and the LiH transition state model at the semiempirical levels are the best choices to predict diastereoselectivity. Unexpectedly, the performance of charge, hydride and LiH transition state models are inferior at the B3LYP level compared to the semiempirical methods in predicting the facial selectivities. On the other hand, the Cieplak type hyperconjugation evaluated using the NBO analysis, and cation complexation model are less reliable despite the fact that these two involve higher (B3LYP/6-31G*) level calculations. The inadequate performance of the charge model, NBO and the cation complexation models were traced to their emphasis on only one or two factors which are responsible for stereodifferentiation and undermining of the other subtle aspects involving a combination of orbital and electrostatic effects. On the other hand, the hydride and LiH transition state models, at semiempirical levels, provide reliable results to model the face-selectivities.

1. Introduction

Induction of face-selectivity in nucleophilic addition to the carbonyl group through remote electronic perturbations is an elegant approach towards stereoselective bond formation. Systems have been designed where the carbonyl group is positioned in an isosteric environment but remote electronic modification through distal substituents can be used to achieve significant levels of diastereoselectivity during nucleophilic additions through face-selection (Scheme 1).[1−3] It is now well recognized that long range electronic effects can play decisive roles in determining
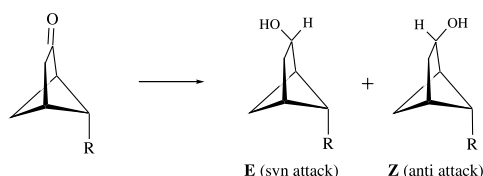
Scheme 1. An example of the nucleophilic addition (all reductions were carried out using NaBH₄ at 0 °C with methanol as the solvent) reaction with a sterically unbiased ketone.

π-facial selectivity. However, precise nature of these effects and how exactly they engender stereo-differentiation during nucleophilic addition is not quite clear, despite many incisive experimental probes and a variety of theoretical models.[4−18] Geometric and orbital distortions, electrostatic effects, different types of specific orbital interactions (Felkin-Anh and Cieplak type) have been analyzed to understand the observed results.[4,5] The Cieplak model highlights the importance of *anti*-periplanar C−C σ bond donations to the σ* of the incipient bond C−H at the transition state.[5] The direction of the pyramidalization of the carbonyl carbon upon metal ion/proton complexation was shown to be a simple predictive model to explain the observed face selectivities.[9] The role of electrostatic interactions, Felkin-Anh model, Houk's LiH transition state model, desymmetrization of the π-orbital, etc. were some of the other attempts put forward to rationalize the face selectivities.[4−7] The computationally attractive hydride and charge models at semi-empirical levels proposed earlier were remarkably successful in explaining the observed face selectivities in a large number of sterically unbiased ketones.[6,10−17] Although, the role of solvent effects on the dynamics of stereoselective processes is well recognized, the theoretical approaches involving solvent effects are scarce.[19]

Modeling face-selectivity has been a challenging task for

theoretical and computational methodologies.[1−9] The quest for providing simple and chemically intuitive models to predict π-facial selectivities continues to engage attention, though it is increasingly becoming evident that in most cases face-selectivities arise through an interplay of various factors acting either concordantly or discordantly. We make an attempt here to consolidate the experimental results reported from nine different probe systems **1R−8R** and **9a−f** and re-evaluate the observed selectivities in terms of the various existing computational models (Scheme 2).[10−17] All reductions were uniformly carried out using NaBH₄ at 0 °C with methanol as the solvent. Considering the importance of the topic, coupled with the lack of a unique reliable predictive model, we undertook a study to critically evaluate the applicability and limitations of various theoretical models. Towards this end, MNDO, AM1 and B3LYP/6-31G* level calculations have been employed to model the π-facial selectivity in these compounds with the charge, hydride and LiH transition state models. Hybrid density functional B3LYP calculations were also performed for the NBO analysis and cation complexation model. In this paper, we attempt to analyze the efficacy of these computational models in predicting the π-facial selectivity in nucleophilic addition reactions to sterically unbiased ketones.
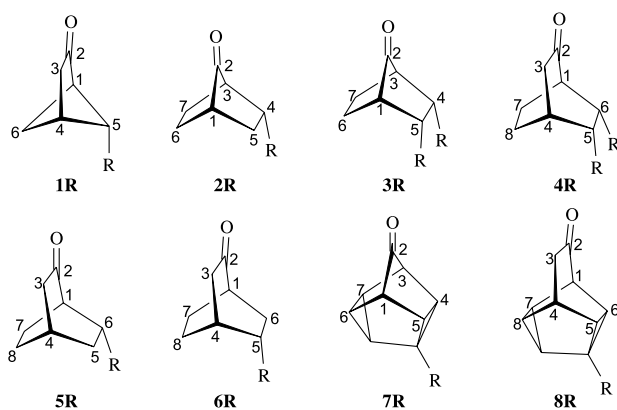
R = CN, COOMe, CCH, CH₂OH, CH₂CH₃ and CHCH₂
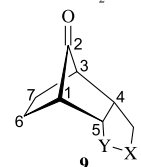
a: X=CH₂ ;   Y=CH₂
b: X=O ;   Y=CH₂
c: X=S ;   Y=CH₂
d: X=S(=O) ; Y=CH₂
e: X=S(=O)O ; Y=CH₂
f: X=O ;   Y=CO

Scheme 2. The nine different probes considered in the study.

2. Methodology

All 54 compounds, **1R−8R** and **9a−f**, selected in the present study, were fully optimized at the B3LYP/6-31G* level and at the semiempirical MNDO[20] and AM1[21] levels. The stationary points thus obtained were characterized by frequency calculations at the semiempirical levels and were confirmed as minima on their respective potential energy surfaces. Various conformers were considered for the compounds with conformationally flexible substituents to locate the global minima at the AM1 level. The transition states corresponding to the LiH addition to the two faces of the carbonyl group were located and characterized as saddle points using the frequency calculations at the semiempirical MNDO and AM1 levels of theory. The location of LiH transition state, charge model and hydride model calculations at B3LYP level were also carried out, but only in those cases (37) where the experimental facial selectivity results are available. NBO analyses were performed using the B3LYP/6-31G* optimized geometries to evaluate the Cieplak type hyperconjugation interactions using the NBO subroutine[22] implemented in the Gaussian 98 program package.[23] Geometry optimizations were also performed on the reactants with a proton complexed to the carbonyl oxygen at the B3LYP/6-31G* level. In the cation complexation model, the face selectivities depend on the direction of the C=O group pyramidalization in the protonated complexes. The semiempirical, AM1 and MNDO, calculations were performed using the MOPAC 2000 program package[24] and the B3LYP calculations were done using the Gaussian 98 suite of programs. The geometric parameters and the nature of the imaginary frequencies were examined using the graphical interface program, MOPLOT.[25]

3. Results and discussion

The results obtained using the charge and hydride models are presented first and are followed by a discussion on the performance of the LiH addition transition state model. In the following sections, the prediction of π-facial selectivity by Cieplak hyperconjugative stabilization, the NBO results, as measured by the interaction energy between the σ-bonds and $\pi^*_{C=O}$ are discussed. The principal dihedral angles of the protonated complexes are given next to examine the performance of the cation complexation model. Finally, a comparison of the predictive abilities of all these computational models is provided.

3.1. Charge and hydride models

The charge and hydride model calculations were carried out by placing a point charge (using sparkles option in MOPAC program package and point charges coupled with the massage keyword in G98) and hydride ion, respectively, 1.4 Å away from the carbonyl carbon on both sides along the trajectory perpendicular to the carbonyl face of the optimized reactant geometries.[6] The preferential facial attack is estimated from the relative energy differences of the two species which are expected to mimic the corresponding putative transition state structures. While the charge model considers exclusively the electrostatic effects, the hydride model takes into account both electrostatic and orbital effects. The predicted face selectivities of the systems under study using the charge and hydride models at the MNDO and AM1 levels are depicted in Table 1. Among the 54 structures considered in the present study, the experimental face selectivity values are available

Table 1. The relative energies (kcal/mol) for *syn* and *anti* face additions calculated using the charge and hydride models at the MNDO and AM1 levels[a] and the experimental diastereoselection

Structure	Charge model				Hydride model				Expt.
	MNDO		AM1		MNDO		AM1		
	syn	*anti*	*syn*	*anti*	*syn*	*anti*	*syn*	*anti*	
1CN	0.26	0.00	0.00	1.85	0.00	0.67	0.00	1.19	75/25
1COOMe	1.65	0.00	0.00	0.56	0.00	0.47	0.00	1.02	66/34
1CCH	2.00	0.00	0.37	0.00	0.04	0.00	0.00	0.38	60/40
1CH$_2$OH	3.95	0.00	3.27	0.00	0.63	0.00	0.23	0.00	48/52
1CH$_2$CH$_3$	4.29	0.00	3.02	0.00	0.78	0.00	0.41	0.00	47/53
1CHCH$_2$	3.06	0.00	3.50	0.00	0.38	0.00	0.68	0.00	44/56
2CN	0.00	1.88	0.00	4.09	0.00	1.40	0.00	1.96	88/12
2COOMe	0.00	0.60	0.00	3.84	0.00	1.26	0.00	2.20	68/32
2CCH	0.88	0.00	0.00	1.05	0.00	0.13	0.00	0.79	69/31
2CH$_2$OH	2.62	0.00	1.25	0.00	0.37	0.00	0.00	0.26	—
2CH$_2$CH$_3$	4.47	0.00	3.28	0.00	1.08	0.00	0.59	0.00	35/65
2CHCH$_2$	3.24	0.00	1.22	0.00	0.84	0.00	0.05	0.00	43/57
3CN	0.00	3.34	0.00	7.73	0.00	2.61	0.00	3.77	—
3COOMe	0.00	1.01	0.00	6.70	0.00	2.22	0.00	4.08	84/16
3CCH	2.04	0.00	0.00	1.57	0.00	0.17	0.00	1.44	—
3CH$_2$OH	6.77	0.00	5.03	0.00	1.39	0.00	0.48	0.00	40/60
3CH$_2$CH$_3$	8.47	0.00	6.77	0.00	2.13	0.00	1.28	0.00	20/80
3CHCH$_2$	6.82	0.00	5.84	0.00	1.71	0.00	1.29	0.00	36/64
4CN	0.00	1.13	0.00	3.73	0.00	1.61	0.00	2.18	—
4COOMe	1.77	0.00	0.00	1.00	0.00	1.72	0.00	2.82	70/30
4CCH	1.89	0.00	0.00	0.51	0.00	0.21	0.00	1.01	—
4CH$_2$OH	4.42	0.00	8.08	0.00	0.95	0.00	0.00	0.81	52/48
4CH$_2$CH$_3$	4.89	0.00	1.75	0.00	1.11	0.00	1.15	0.00	39/61
4CHCH$_2$	5.16	0.00	4.09	0.00	0.90	0.00	0.51	0.00	50/50
5CN	0.00	0.66	0.00	4.59	0.00	0.88	0.00	0.98	—
5COOMe	0.45	0.00	0.00	7.24	0.00	0.60	0.00	0.75	65/35
5CCH	1.30	0.00	0.00	2.90	0.03	0.00	0.00	0.07	—
5CH$_2$OH	3.86	0.00	0.80	0.00	1.00	0.00	0.33	0.00	—
5CH$_2$CH$_3$	3.77	0.00	0.87	0.00	0.89	0.00	0.87	0.00	—
5CHCH$_2$	3.56	0.00	0.46	0.00	0.88	0.00	1.01	0.00	—
6CN	0.00	0.90	0.13	0.00	0.00	0.89	0.00	1.41	—
6COOMe	0.00	0.16	1.94	0.00	0.00	0.77	0.00	1.53	62/38
6CCH	0.41	0.00	1.99	0.00	0.00	0.32	0.00	1.06	—
6CH$_2$OH	1.31	0.00	3.89	0.00	0.00	0.16	0.00	0.88	—
6CH$_2$CH$_3$	3.04	0.00	3.13	0.00	0.27	0.00	0.00	0.45	—
6CHCH$_2$	1.60	0.00	3.41	0.00	0.03	0.00	0.00	0.54	—
7CN	0.00	3.99	0.00	4.53	0.00	1.65	0.00	1.67	84/16
7COOMe	0.00	4.89	0.00	5.02	0.00	1.70	0.00	1.89	79/21
7CCH	0.00	2.17	0.00	3.13	0.00	0.93	0.00	1.18	76/24
7CH$_2$OH	0.00	1.53	0.00	2.45	0.00	0.81	0.00	0.96	56/44
7CH$_2$CH$_3$	0.00	0.95	0.00	0.55	0.00	0.55	0.00	0.32	48/52
7CHCH$_2$	0.00	1.37	0.00	1.62	0.00	0.72	0.00	0.68	60/40
8CN	0.00	1.82	0.00	1.17	0.00	0.81	0.00	0.71	59/41
8COOMe	0.00	1.43	0.00	1.55	0.00	0.69	0.00	0.52	59/41
8CCH	0.00	1.08	0.00	1.29	0.00	0.48	0.00	0.44	57/43
8CH$_2$OH	0.35	0.00	0.00	0.01	0.05	0.00	0.00	0.13	53/47
8CH$_2$CH$_3$	0.00	0.58	0.00	0.01	0.00	0.31	0.00	0.08	—
8CHCH$_2$	0.00	0.46	0.00	0.58	0.00	0.28	0.00	0.26	57/43
9a	6.41	0.00	3.93	0.00	1.20	0.00	0.34	0.00	25/75
9b	4.58	0.00	0.70	0.00	0.25	0.00	0.00	0.72	47/53
9c	4.05	0.00	1.54	0.00	0.26	0.00	0.00	0.36	44/56
9d	3.65	0.00	2.67	0.00	0.18	0.00	0.00	0.14	42/58
9e	1.30	0.00	0.00	3.12	0.00	1.02	0.00	2.01	53/47
9f	0.76	0.00	0.00	4.82	0.00	1.35	0.00	2.46	84/16

[a] A value of 0.00 denotes a preference of the corresponding side attack.

for 38 substrates and enable an assessment of the predictive ability of a given computational model and are collected in the same Table. The B3LYP relative energies of the charge and hydride model transition states of the compounds for which experimental data are available are depicted in Table 2.[26]

Charge model at AM1 level reproduces the observed diastereoselection for all **1R** compounds except when R=CCH, whereas MNDO uniformly predicts *anti* addition for all **1R** compounds, which results in incorrect prediction in a few cases. On the other hand, hydride model at both MNDO and AM1 levels reproduces the experimental results in a fairly satisfactory manner. Importantly, the trends in the computed energy difference between the *syn* and *anti* attack correlate well with the observed selectivity. Charge model with AM1 method reproduces the π-facial selectivity of **2R** for all the substituents, but the MNDO level fails to account

Table 2. The relative energies (kcal/mol) for *syn* and *anti* face additions calculated using the charge, hydride and LiH TS models at the B3LYP/6-31G* level[a]

Structure	Charge		Hydride		LiH	
	syn	*anti*	*syn*	*anti*	*syn*	*anti*
1CN	0.00	3.70	0.00	1.28	0.00	1.16
1COOMe	0.00	2.81	1.95	0.00	0.00	0.46
1CCH	0.00	3.17	0.15	0.00	0.00	0.41
1CH$_2$OH	0.00	0.76	1.03	0.00	0.14	0.00
1CH$_2$CH$_3$	0.00	2.00	1.89	0.00	0.09	0.00
1CHCH$_2$	0.00	3.40	1.46	0.00	0.00	0.34
2CN	0.00	5.51	0.00	2.66	0.00	2.24
2COOMe	0.00	4.75	0.00	3.69	0.00	1.57
2CCH	0.00	4.82	0.07	0.00	0.00	1.05
2CH$_2$CH$_3$	0.00	2.77	4.51	0.00	0.38	0.00
2CHCH$_2$	0.00	3.99	0.00	0.63	1.08	0.00
3COOMe	0.00	7.87	0.00	3.16	0.00	1.65
3CH$_2$OH	0.00	3.07	4.52	0.00	0.14	0.00
3CH$_2$CH$_3$	0.00	5.43	7.82	0.00	0.51	0.00
3CHCH$_2$	0.00	5.99	9.56	0.00	0.17	0.00
4COOMe	0.00	0.00	0.00	0.00	0.00	1.42
4CH$_2$OH	0.00	0.91	0.00	1.84	0.29	0.00
4CH$_2$CH$_3$	0.00	1.58	6.52	0.00	0.27	0.00
5COOMe	0.00	2.19	0.10	0.00	0.00	2.08
6COOMe	0.00	1.73	0.00	1.56	0.00	0.39
7CN	0.00	0.00	0.00	8.57	0.00	0.78
7COOMe	1.14	0.00	0.00	7.03	0.00	0.15
7CCH	0.06	0.00	0.00	6.21	0.00	0.46
7CH$_2$OH	1.26	0.00	0.21	0.00	0.00	0.31
7CH$_2$CH$_3$	0.00	0.37	0.25	0.00	0.06	0.00
7CHCH$_2$	0.32	0.00	0.00	3.79	0.00	0.09
8CN	0.00	0.79	0.00	2.62	0.00	0.35
8COOMe	1.17	0.00	0.00	0.30	0.49	0.00
8CCH	0.00	0.55	0.00	1.64	0.00	0.08
8CH$_2$OH	0.00	0.08	0.20	0.00	0.02	0.00
8CHCH$_2$	0.00	0.41	0.00	1.58	0.11	0.00
9a	0.00	3.76	7.45	0.00	0.87	0.00
9b	0.00	5.02	4.49	0.00	0.00	0.15
9c	0.00	6.43	2.65	0.00	0.00	0.78
9d	0.00	5.48	0.63	0.00	0.00	0.93
9e	0.00	9.09	0.00	1.22	0.00	2.44
9f	0.00	5.48	2.19	0.00	0.00	1.15

[a] A value of 0.00 denotes a preference of the corresponding side attack.

Table 3. The relative energies of the LiH addition transition[a] states from the *syn* and *anti* side obtained at MNDO and AM1 levels. All values are given in kcal/mol

Structure	Transition state			
	MNDO		AM1	
	syn	*anti*	*syn*	*anti*
1CN	0.00	0.26	0.00	0.58
1COOMe	0.05	0.00	0.00	0.34
1CCH	0.14	0.00	0.00	0.17
1CH$_2$OH	0.48	0.00	0.27	0.00
1CH$_2$CH$_3$	0.32	0.00	0.24	0.00
1CHCH$_2$	0.30	0.00	0.24	0.00
2CN	0.00	0.55	0.00	0.93
2COOMe	0.00	0.37	0.00	0.80
2CCH	0.00	0.00	0.00	0.42
2CH$_2$OH	0.20	0.00	0.03	0.00
2CH$_2$CH$_3$	0.31	0.00	0.20	0.00
2CHCH$_2$	0.25	0.00	0.55	0.00
3CN	0.00	1.07	0.00	1.87
3COOMe	0.00	0.55	0.00	1.57
3CCH	0.01	0.00	0.00	0.83
3CH$_2$OH	0.57	0.00	0.29	0.00
3CH$_2$CH$_3$	0.65	0.00	0.47	0.00
3CHCH$_2$	0.53	0.00	0.22	0.00
4CN	0.00	0.76	0.00	1.18
4COOMe	0.00	0.22	0.00	0.69
4CCH	0.01	0.00	0.00	0.50
4CH$_2$OH	0.59	0.00	0.61	0.00
4CH$_2$CH$_3$	0.49	0.00	0.35	0.00
4CHCH$_2$	0.39	0.00	0.21	0.00
5CN	0.00	0.46	0.00	0.90
5COOMe	0.00	0.11	0.00	0.74
5CCH	0.01	0.00	0.00	0.49
5CH$_2$OH	0.48	0.00	0.27	0.00
5CH$_2$CH$_3$	0.30	0.00	0.12	0.00
5CHCH$_2$	0.28	0.00	0.03	0.00
6CN	0.00	0.33	0.00	0.32
6COOMe	0.00	0.21	0.00	0.13
6CCH	0.00	0.01	0.00	0.04
6CH$_2$OH	0.08	0.00	0.16	0.00
6CH$_2$CH$_3$	0.14	0.00	0.25	0.00
6CHCH$_2$	0.12	0.00	0.15	0.00
7CN	0.00	0.43	0.00	0.45
7COOMe	0.00	0.33	0.00	0.32
7CCH	0.00	0.15	0.00	0.19
7CH$_2$OH	0.00	0.22	0.00	0.30
7CH$_2$CH$_3$	0.00	0.07	0.00	0.02
7CHCH$_2$	0.00	0.07	0.00	0.08
8CN	0.00	0.29	0.00	0.28
8COOMe	0.00	0.20	0.00	0.14
8CCH	0.00	0.10	0.00	0.11
8CH$_2$OH	0.00	0.01	0.00	0.02
8CH$_2$CH$_3$	0.00	0.04	0.08	0.00
8CHCH$_2$	0.00	0.03	0.00	0.04
9a	0.47	0.00	0.17	0.00
9b	0.10	0.00	0.00	0.36
9c	0.07	0.00	0.00	0.29
9d	0.18	0.00	0.00	0.21
9e	0.00	0.49	0.00	1.28
9f	0.00	0.47	0.00	1.02

[a] A value of 0.00 denotes a preference of the corresponding side attack.

for the *syn* selectivity of **2CCH**. The results obtained with hydride model at both MNDO and AM1 methods are in good agreement with experimental results.

In substrates **3R**, charge and hydride models at both AM1 and MNDO levels reproduce correctly the experimentally observed facial preferences. All methods predict uniform *syn* preference for **3CN** and **4CN**, for which the experimental data is not available. Similarly, for **3CCH**, where the experimental selectivity is not known, hydride and AM1 charge models predict *syn* selectivity whereas MNDO charge model predicts *anti* addition. In the case of **4R**, hydride model at AM1 level is relatively more satisfactory but the loss of selectivity for **4CHCH$_2$** could not be reproduced. The experimental selectivities for **5COOMe** and **6COOMe** are reproduced by both hydride and charge models at the AM1 level. It is also predicted that for **5CN** and **6CN**, the nucleophile would prefer *syn* attack compared to *anti* attack. Similarly, computation reveals that **5CCH** and **6CCH** favor *syn* addition, whereas **5CH$_2$OH**, **5CH$_2$CH$_3$** and **5CHCH$_2$** prefer *anti* addition. For **6R**, charge and hydride models predict opposite selectivities in most of the cases.

All the methods applied here correctly reproduce the experimentally observed *syn* preference, except for **7CH$_2$CH$_3$**, and encouragingly the computed magnitudes of the relative energies match with the ratios highlighting the superiority of hydride model. However, the marginal *anti* preference of **7CH$_2$CH$_3$** could not be reproduced at any level of theory albeit the magnitude of the computed energy

differences is negligibly small. The consistently observed *syn* selectivity of system **8R** with any type of substituent is supported by the computed results.

3.2. LiH addition transition state model

LiH addition transition states have been widely used to model the real transition state in nucleophilic addition to ketones.[7] The transition states were obtained by approaching the Li–H, parallel to the C=O along the plane, where H and Li are oriented towards C and O of carbonyl respectively on either side of the π-plane. Tables 2 and 3 depict the energy differences between the *syn* and *anti* transition states obtained at the DFT, and the semiempirical levels of theory respectively; comparison with the available experimental results points to an excellent predictive ability of this approach especially at the semiempirical levels. The relative energies of the *syn* and *anti* side attacks of LiH to **1R** computed at the AM1 level explain the diastereoselection, whereas performance at the MNDO level is slightly less satisfactory. However, the qualitative trends of the relative energy differences correlate well with the experimental values. Similar to **1R**, while AM1 could reproduce the experimental selectivity for **2R**, the MNDO level could not differentiate the two faces as the energies of *syn* and *anti* transition states are the same for **2CCH**. *anti*-Selectivity is predicted for **2CH₂OH** by both AM1 and MNDO levels, for which the experimental data is not available. However, both AM1 and MNDO levels reproduce the observed diastereoselection in **2R**. Experimental results on **3CN**, **4CN**, **5CN** and **6CN** are not known; LiH transition states predict preferential *syn* attack at both levels, similar to the charge and hydride models. The relative energies of the *syn* and *anti* LiH transition states of **3R** very well account for the observed selectivities in **3R**. Encouragingly, both economically attractive MNDO and AM1 levels perform equally well for all probe systems except **1R** and **9a–f**. Similar to the situation in the charge and hydride models, the performance of the hybrid density functional theory level is inferior compared to that of the semiempirical methods.

3.3. NBO analysis

The second order perturbative analysis in the NBO procedure is used to estimate the Cieplak type hyperconjugative effect, namely the interaction energies between the σ of the C–C bond *anti*-periplanar to the incipient C–H bond being formed and the π* of the carbonyl.[8] Table 4 gives the interaction energies between all the Cieplak type interactions (involving the primary anti-periplanar σ_{C-C} and other involved σ bonds) with $\pi^*_{C=O}$ from the *syn* and *anti* sides obtained at the B3LYP/6-31G* level. The NBO analysis could reproduce the experimental selectivities only in about 40% of the cases. The highly electron withdrawing CN substituted compounds are expected to show smaller interaction energies between the σ of *syn* C–C bond and the $\pi^*_{C=O}$ compared to those between the σ of *anti* C–C bond and the $\pi^*_{C=O}$. But, in **1CN** and **2CN**, the interaction energies in the *syn* side C–C bond are greater than those from the *anti* side C–C bond indicating an *anti* preference. Also, the trend followed by the interaction energies does not correlate well with the experimental data.[27]

Table 4. The interaction energies (in kcal/mol) between all the Cieplak type interactions with $\pi^*_{C=O}$ using NBO along with the principle dihedral angles (in degrees) in the proton complexed reactants obtained at the B3LYP/6-31G* level.[a] All values are given in degrees

Structure	NBO (σ–π*)		Cation complexation model			
	syn	*anti*	*syn*		*anti*	
			D1	D2	D3	D4
1CN	9.19	8.75	138.0	—	136.7	—
1COOMe	9.47	8.82	133.4	—	141.5	—
1CCH	9.48	8.85	132.1	—	143.3	—
1CH₂OH	9.32	9.19	135.0	—	139.4	—
1CH₂CH₃	9.37	9.14	130.4	—	144.4	—
1CHCH₂	9.67	8.94	130.7	—	144.8	—
2CN	7.33	6.92	128.9	128.5	120.2	121.2
2COOMe	7.33	7.40	124.9	127.5	123.3	122.6
2CCH	7.47	7.00	123.0	123.1	126.4	126.7
2CH₂CH₃	7.40	7.25	116.6	120.5	131.3	129.6
2CHCH₂	7.29	7.43	120.1	125.4	128.2	125.0
3COOMe	7.63	7.23	127.4[b]	124.0[b]	120.0[b]	124.0[b]
3CH₂OH	7.35	7.27	115.6[b]	114.7[b]	132.6[b]	132.6[b]
3CH₂CH₃	7.59	7.08	114.2[b]	112.3[b]	133.7[b]	135.9[b]
3CHCH₂	7.81	6.70	112.1[b]	112.9[b]	135.9[b]	135.2[b]
4COOMe	6.74	8.08	121.2	—	122.0	—
4CH₂OH	7.16	8.10	118.1	—	124.7	—
4CH₂CH₃	8.63	6.67	114.7	—	128.8	—
5COOMe	7.68	7.63	131.1	—	112.9	—
6COOMe	7.27	7.83	125.4	—	119.6	—
7CN	7.11	8.09	147.1	146.3	105.9	106.9
7COOMe	7.09	8.26	146.6	145.8	106.6	107.4
7CCH	7.30	8.10	147.0	146.2	106.2	107.1
7CH₂OH	7.92	7.78	105.8	106.7	147.7	146.9
7CH₂CH₃	7.87	7.78	107.1	107.9	146.4	145.6
7CHCH₂	7.37	8.09	144.9	144.1	108.4	109.2
8CN	7.39	7.48	142.1	—	122.9	—
8COOMe	7.38	7.52	122.9	—	126.4	—
8CCH	7.46	7.53	120.4	—	128.7	—
8CH₂OH	7.54	7.53	118.9	—	130.4	—
8CHCH₂	7.52	7.52	116.9	—	132.5	—
9a	7.53	6.92	111.1	110.5	135.9	136.7
9b	7.52	6.95	113.7	113.4	133.5	133.7
9c	7.23	7.06	116.4	116.1	130.3	130.5
9d	7.08	7.03	110.4	110.0	136.6	136.9
9e	7.13	7.08	126.1	126.1	120.7	120.7
9f	7.59	6.84	121.3	116.3	127.0	131.1

[a] If D1>D3 and D2>D4, syn attack is preferred and if D3>D1 and D4>D2, *anti* attack is preferred. For **1R**, D1=∠O-2-1-5 and D3=∠O-2-1-6; for systems **2R**, **3R**, **7R** and **9a–f**, D1=∠O-2-1-5, D2=∠O-2-3-4, D3=∠O-2-1-6 and D4=∠O-2-3-7; and for systems **4R**, **5R**, **6R** and **8R**, D1=∠O-2-1-6 and D3=∠O-2-1-7. Here, O denotes the carbonyl carbon, where the nucleophilic addition occurs.
[b] Taken from Ref. 28.

3.4. Cation complexation model

This approach critically analyzes the pyramidalization of the carbonyl carbon or the tilting of the carbonyl group towards one of the sides upon complexation with proton or cations like Li⁺ and Na⁺.[9] According to this model, if the carbonyl group is tilted towards one of the sides upon complexation, the nucleophilic addition will be preferred from the other side. The principal dihedral angles in the proton complexed reactants, which estimate the pyramidalization of the carbonyl carbon upon proton complexation, obtained at the B3LYP/6-31G* level are given in Table 4. Calculations were done only on those systems where the experimental data are available. The atom numbering used in the Table is illustrated in Scheme 2. This model reproduces the selectivity in about 70% of the
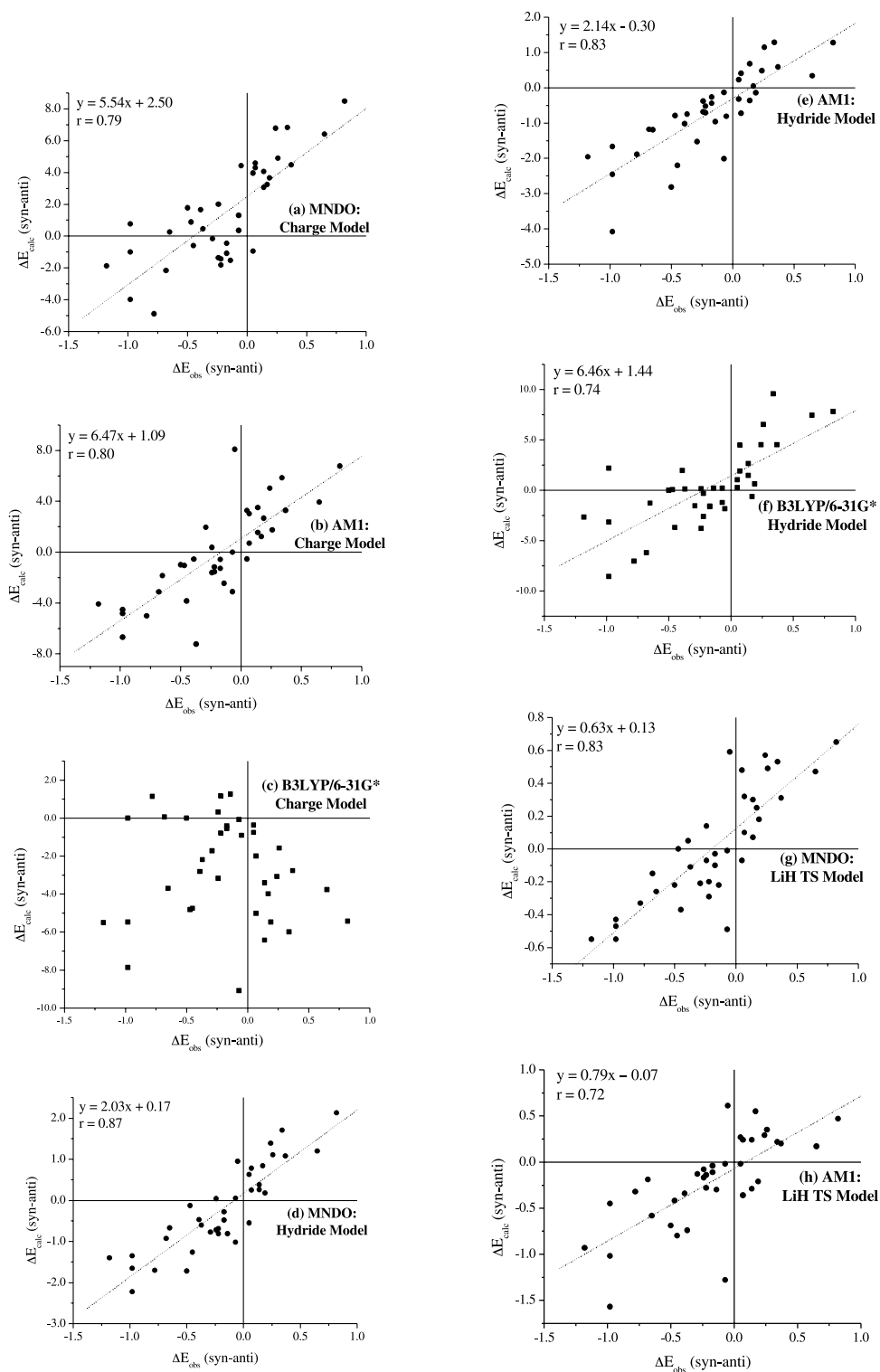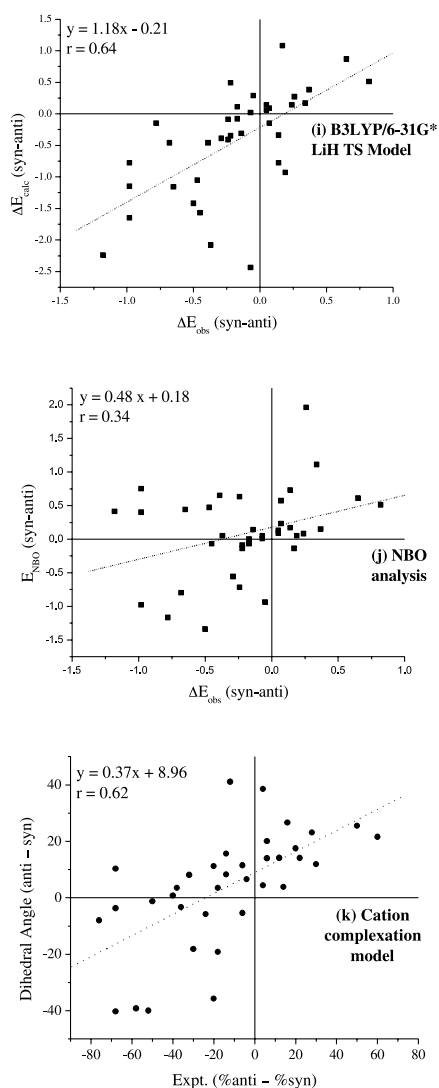
Figure 1 (*legend opposite*)

experimental cases, however, a closer look reveals that the degree of tilting of the carbonyl group does not seem to have any correlation with the extent of selectivity. For example, the experimental results indicate that **9e** has marginal preference for *syn* (*syn*:*anti* ratio is 53:47), this model correctly predicts *syn* selectivity. However, **9f** is observed to undergo preferential *syn* addition (*syn*:*anti* ratio is 84:16); the cation complexation model predicts a preferential *anti* attack. Thus the cation complexation model, which

considers primarily one aspect of all the possible factors, does not seem to have a reliable predictive ability, especially in the presence of overriding electrostatic and orbital effects around the transition state region along the trajectory of the nucleophilic attack.

3.5. Assessing the predictive ability

The foregoing discussion highlights the intricacies of the

$y = 1.18x - 0.21$
$r = 0.64$

(i) B3LYP/6-31G* LiH TS Model

ΔE_{calc} (syn-anti)

ΔE_{obs} (syn-anti)

$y = 0.48\,x + 0.18$
$r = 0.34$

(j) NBO analysis

E_{NBO} (syn-anti)

ΔE_{obs} (syn-anti)

$y = 0.37x + 8.96$
$r = 0.62$

(k) Cation complexation model

Dihedral Angle (anti – syn)

Expt. (%anti – %syn)

Figure 1. The correlation of the experimental face selectivities with the predicted selectivity values by charge model (a, b, c), hydride model (d, e, f), LiH transition state model (g, h, i), NBO analysis (j) and cation complexation model (k). The '*r*' values corresponding to each of the linear fit are given in the corresponding figures.

problem and it is necessary to ascertain the predictive ability of a given model in quantitative terms. The relative performance of the eight theoretical models is assessed through a comparison of the predicted values with the available experimental results, Figure 1.

Figure 1a–k gives the correlation of the observed and the computed facial selectivities obtained using various computational models discussed above. In all the figures, the points, which lie within the diagonal boxes (lower left side to upper right side), provide the correct qualitative picture. The linear equations employed to fit the data of the computed selectivities with the experimental ones along with the correlation coefficients are given in Figure 1. A quick look at the figures indicate that while most points lie within the correct region, the number of points present outside the boxes is significant for the NBO and cation complexation models. The correlation constant (*r*) values for the linear fits given in the corresponding figures indicate the quality of the linear fit of each of the method and the

intercept value in the linear equation gives the deviation from the perfect prediction. The comparison of the '*r*' values indicates that the hydride model and the LiH TS model, especially at the MNDO level, are better compared to the other models. A quick look at Figure 1 indicates that the performance of hydride and LiH transition state models is consistently better than that of charge model. Such results can be understood due to the complete neglect of orbital interactions in the charge model, while the hydride and LiH transition state models incorporate both charge and overlap effects. However, it is quite surprising to see that the performance of generally more reliable B3LYP method is clearly inferior to both the semiempirical methods. NBO analysis fails in predicting both the direction of the selectivity and the extent of selectivity. Even though the cation complexation model is successful in predicting the facial preferences in about 70% of the cases, the trends in the predicted selectivity do not match with the experimental data.

While predicting the direction of selectivity is a crucial first step for any model, estimation of the extent of selectivity is also an equally important aspect. The predictive abilities of molecular modeling approaches need not have a correct basis to provide data that agrees with experiments and chance correlations could not be avoided.[29] Thus, both factors namely the prediction of the direction and the extent have to be taken to ascertain the credibility of a given model. Thus, the quality of linear correlation between the *syn/anti* preferences and the parameters chosen to distinguish the preferences is drawn to assess the reliability of the models. Here, the correlation coefficient value *r* gives an idea about the ability of the methods to yield reasonable trends. Thus, the statistical analysis indicates that the hydride model were the best choices. However, the correlation coefficient values of 0.62 and 0.34 for the cation complexation and NBO analyses indicate the absolute limitations of these models in predicting the extent of selectivity. The intercept value close to zero and the correlation coefficient closer to unity gauges the performance of a given model. Therefore, the analysis quantifies the better performance of hydride and LiH transition state models compared to the rest.

4. Conclusions

The present study reports semiempirical (MNDO and AM1) and hybrid density functional theory (B3LYP) calculations on several probe systems wherein the two faces of the carbonyl group are in isosteric environment, but are electronically differentiated. The predictive ability of several methods such as the hydride model, the charge model, the LiH transition state model, Cieplak hyperconjugation effect estimated by NBO analysis and cation complexation model are critically analyzed in both qualitative and quantitative terms. Our studies reveal that the hydride model, at both MNDO and AM1 levels, is a sensible way to obtain quick insights into the π-facial selectivity in the nucleophilic additions to sterically unbiased ketones. Clearly, hydride, LiH transition state and charge models perform better at the semiempirical levels compared to the computationally expensive B3LYP level of theory, a result which is difficult to comprehend. The performance of the

LiH addition transition state model is comparable to that of the hydride model. The computationally expensive calculations of NBO and cation complexation models are aimed at singling out one or two key factors, which are responsible for the stereodifferentiation. Nonetheless, even at the B3LYP level, the predictive ability of the hydride and LiH transition state models are better compared to the charge model, Cieplak type hyperconjugation interactions from NBO analysis and cation complexation model. However, considering the fact that the preference for facial selectivity depends on an intricate mix of mutually independent and subtle electronic and electrostatic factors, any model that relies heavily on a single aspect is not expected to yield reliable results. The superior performance of the hydride model to predict the π-facial selectivities over the other models in this class of compounds indicates its ability to judiciously accommodate the cumulative effects due to orbital and electrostatic origins. Thus, the present study proposes that hydride model is a reliable and economic model to estimate the π-facial selectivity of nucleophilic addition to sterically unbiased ketones.

References and notes

1. *Chem. Rev.* **1999**, *99*(5), 1067–1480. (b) Mehta, G.; Chandrasekhar, J. *Chem. Rev.* **1999**, *99*, 1437–1468.
2. Li, H.; le Noble, W. J. *Recl. Trav. Chim. Pays-Bas.* **1992**, *111*, 199–210.
3. Gung, B. W. *Tetrahedron* **1996**, *52*, 5263–5301.
4. (a) Huet, J.; Bernard, Y.-M.; Anh, N. T.; Seyden-Penne, J. *Tetrahedron Lett.* **1976**, 159–162. (b) Anh, N. T.; Eisenstein, O. *Noveau J. Chem.* **1977**, *1*, 61–70. (c) Anh, N. T. *Top. Curr. Chem.* **1980**, *88*, 145–162.
5. (a) Cieplak, A. S. *J. Am. Chem. Soc.* **1981**, *103*, 4540–4552. (b) Cieplak, A. S. *Chem. Rev.* **1999**, *99*, 1265–1336.
6. Ganguly, B.; Chandrasekhar, J.; Khan, F. A.; Mehta, G. *J. Org. Chem.* **1993**, *58*, 1734–1739.
7. (a) Kaufmann, E.; Schleyer, P. v. R.; Houk, K. N.; Wu, Y.-D. *J. Am. Chem. Soc.* **1985**, *107*, 5560–5562. (b) Wu, Y.-D.; Houk, K. N. *J. Am. Chem. Soc.* **1987**, *109*, 908–910. (c) Paddon-Row, M. N.; Wu, Y.-D.; Houk, K. N. *J. Am. Chem. Soc.* **1992**, *114*, 10638–10639.
8. Senju, T.; Tomoda, S. *Chem. Lett.* **1997**, 431–432.
9. Jeyaraj, D. A.; Yadav, A.; Yadav, V. K. *Tetrahedron Lett.* **1997**, *38*, 4483–4486.
10. Mehta, G.; Singh, S. R.; Gagliardini, V.; Priyakumar, U. D.; Sastry, G. N. *Tetrahedron Lett.* **2001**, *42*, 8527–8530.
11. Mehta, G.; Khan, F. A.; Adcock, W. *J. Chem. Soc., Perkin Trans. 2* **1995**, 2189–2190.
12. Mehta, G.; Khan, F. A. *J. Am. Chem. Soc.* **1990**, *112*, 6140–6142.
13. Mehta, G.; Khan, F. A.; Ganguly, B.; Chandrasekhar, J. *J. Chem. Soc., Chem. Commun.* **1992**, 1711–1712.
14. Mehta, G.; Khan, F. A. *J. Chem. Soc., Perkin Trans. 1* **1993**, 1727–1728.
15. Mehta, G.; Ravikrishna, C.; Ganguly, B.; Chandrasekhar, J. *J. Chem. Commun.* **1997**, 75–76.
16. Mehta, G.; Ravikrishna, C.; Kalyanaraman, P.; Chandrasekhar, J. *J. Chem. Soc., Perkin Trans. 1* **1998**, 1895–1897.
17. Mehta, G.; Gagliardini, V.; Priyakumar, U. D.; Sastry, G. N. *Tetrahedron Lett.* **2002**, *43*, 2487–2490.
18. (a) Li, H.; Mehta, G.; Padma, S.; le Noble, W. J. *J. Org. Chem.* **1991**, *56*, 2006. (b) Mehta, G.; Khan, F. A.; Mohal, N.; Namboothiri, I. N. N.; Kalyanaraman, P.; Chandrasekhar, J. *J. Chem. Soc., Perkin Trans. 1* **1996**, 2665–2667. (c) Mehta, G.; Khan, F. A.; Ganguly, B.; Chandrasekhar, J. *J. Chem. Soc., Perkin Trans. 2* **1994**, 2275–2277. (d) Mehta, G.; Khan, F. A.; Lakshmi, K. A. *Tetrahedron Lett.* **1992**, *33*, 7977–7980. (e) Mehta, G.; Khan, F. A. *Tetrahedron Lett.* **1992**, *33*, 3065–3068. (f) Mehta, G.; Singh, S. R.; Priyakumar, U. D.; Sastry, G. N. *Tetrahedron Lett.* **2003**, *44*, 3101–3104. (g) Gonikberg, E. M.; le Noble, W. J. *J. Org. Chem.* **1995**, *60*, 7751–7755.
19. (a) Cainelli, G.; Giacomini, D.; Galletti, P. *Chem. Commun.* **1999**, 567–572. (b) Cieplak, A. S.; Wiberg, K. B. *J. Am. Chem. Soc.* **1992**, *114*, 9226–9227.
20. Dewar, M. J. S.; Theil, W. *J. Am. Chem. Soc.* **1977**, *99*, 4899–4907.
21. Dewar, M. J. S.; Zoebisch, Z.; Healy, E. F.; Stewart, J. J. P. *J. Am. Chem. Soc.* **1985**, *107*, 3902–3909.
22. Glendening, E. D.; Reed. A. E.; Carpenter, J. E.; Weinhold, F. *NBO Version 3.1.*
23. Frisch, M. J.; Trucks, G. W.; Schlegel, H. B.; Scuseria, G. E.; Robb, M. A.; Cheeseman, J. R.; Zakrzewski, V. G.; Montgomery, Jr., J. A.; Stratmann, R. E.; Burant, J. C.; Dapprich, S.; Millam, J. M.; Daniels, A. D.; Kudin, K. N.; Strain, M. C.; Farkas, O.; Tomasi, J.; Barone, V.; Cossi, M.; Cammi, R.; Mennucci, B.; Pomelli, C.; Adamo, C.; Clifford, S.; Ochterski, J.; Petersson, G. A.; Ayala, P. Y.; Cui, Q.; Morokuma, K.; Rega, N.; Salvador, P.; Dannenberg, J. J.; Malick, D. K.; Rabuck, A. D.; Raghavachari, K.; Foresman, J. B.; Cioslowski, J.; Ortiz, J. V.; Baboul, A. G.; Stefanov, B. B.; Liu, G.; Liashenko, A.; Piskorz, P.; Komaromi, I.; Gomperts, R.; Martin, R. L.; Fox, D. J.; Keith, T.; Al-Laham, M. A.; Peng, C. Y.; Nanayakkara, A.; Challacombe, M.; Gill, P. M. W.; Johnson, B.; Chen, W.; Wong, M. W.; Andres, J. L.; Gonzalez, C.; Head-Gordon, M.; Replogle, E. S.; Pople, J. A. *Gaussian 98, Revision A.11.2*; Gaussian, Inc.: Pittsburgh PA, 2001.
24. Stewart, J. J. P. *MOPAC 2000 ver. 1.06*; Fujitsu Ltd.: Tokyo, Japan, 1999.
25. Bally, T.; Albrecht, B.; Matzinger, S.; Sastry, G. M. *Moplot 3.2*; University of Fribourg, 1997.
26. Charge model calculations with a point charge of −0.5 at the B3LYP level, yielded results identical to that of unit negative charge.
27. NBO analyses were also performed on the hydride model transition states at the B3LYP level so that the interaction between the antibonding σ-orbital of the incipient C–H bond and the antiperiplanar bonding orbital from syn and anti sides could be compared.
28. (a) Yadav, V. K.; Balamurugan, R. *J. Chem. Soc., Perkin Trans. 2* **2001**, 1–2. (b) Yadav, V. K. *J. Org. Chem.* **2001**, *66*, 2501–2502.
29. (a) Menger, F. M. *Proc. Natl. Acad.Sci. U. S. A* **2002**, *99*, 2502–4818. (b) Jensen, F. *Introduction to computational chemistry*; Wiley: England, 1999.